Earth and Planetary Science Letters 450 (2016) 392–405

Contents lists available at ScienceDirect

Earth and Planetary Science Letters

www.elsevier.com/locate/epsl

Cyclostratigraphy and eccentricity tuning of the early Oligocene through early Miocene (30.1–17.1 Ma): *Cibicides mundulus* stable oxygen and carbon isotope records from Walvis Ridge Site 1264

Diederik Liebrand [a,*], Helen M. Beddow [b], Lucas J. Lourens [b], Heiko Pälike [a,c], Isabella Raffi [d], Steven M. Bohaty [a], Frederik J. Hilgen [b], Mischa J.M. Saes [b], Paul A. Wilson [a], Arnold E. van Dijk [b], David A. Hodell [e], Dick Kroon [f], Claire E. Huck [a], Sietske J. Batenburg [g,h]

[a] National Oceanography Centre Southampton, University of Southampton, Waterfront Campus, European Way, Southampton SO14 3ZH, United Kingdom
[b] Department of Earth Sciences, Faculty of Geosciences, Utrecht University, Budapestlaan 4, 3584 CD Utrecht, The Netherlands
[c] MARUM–Center for Marine Environmental Sciences, University of Bremen, Leobener Strasse, 28359 Bremen, Germany
[d] Dipartimento di Ingegneria e Geologia (InGeo), Università degli Studi "G. d'Annunzio" di Chieti–Pescara, Campus Universitario, Via dei Vestini 31, 66013 Chieti Scalo, Italy
[e] Department of Earth Sciences, University of Cambridge, Downing Street, Cambridge CB2 3EQ, United Kingdom
[f] School of GeoSciences, Grant Institute, University of Edinburgh, King's Buildings, James Hutton Road, Edinburgh, EH9 3FE, United Kingdom
[g] Institute of Geosciences, Goethe-University Frankfurt am Main, Altenhöferallee 1, 60438 Frankfurt, Germany
[h] Department of Earth Sciences, University of Oxford, South Parks Road, Oxford OX1 3AN, United Kingdom

ARTICLE INFO

Article history:
Received 8 February 2016
Received in revised form 1 June 2016
Accepted 5 June 2016
Available online 30 June 2016
Editor: M. Frank

Keywords:
integrated stratigraphy
palaeoclimatology
Oligocene–Miocene transition
astronomical climate forcing
Ocean Drilling Program Site 1264 (Walvis Ridge)
Antarctic ice sheet

ABSTRACT

Few astronomically calibrated high-resolution (≤5 kyr) climate records exist that span the Oligocene–Miocene time interval. Notably, available proxy records show responses varying in amplitude at frequencies related to astronomical forcing, and the main pacemakers of global change on astronomical time-scales remain debated. Here we present newly generated X-ray fluorescence core scanning and benthic foraminiferal stable oxygen and carbon isotope records from Ocean Drilling Program Site 1264 (Walvis Ridge, southeastern Atlantic Ocean). Complemented by data from nearby Site 1265, the Site 1264 benthic stable isotope records span a continuous ~13-Myr interval of the Oligo-Miocene (30.1–17.1 Ma) at high resolution (~3.0 kyr). Spectral analyses in the stratigraphic depth domain indicate that the largest amplitude variability of all proxy records is associated with periods of ~3.4 m and ~0.9 m, which correspond to 405- and ~110-kyr eccentricity, using a magnetobiostratigraphic age model. Maxima in $CaCO_3$ content, $\delta^{18}O$ and $\delta^{13}C$ are interpreted to coincide with ~110 kyr eccentricity minima. The strong expression of these cycles in combination with the weakness of the precession- and obliquity-related signals allow construction of an astronomical age model that is solely based on tuning the $CaCO_3$ content to the nominal (La2011_ecc3L) eccentricity solution. Very long-period eccentricity maxima (~2.4-Myr) are marked by recurrent episodes of high-amplitude ~110-kyr $\delta^{18}O$ cycles at Walvis Ridge, indicating greater sensitivity of the climate/cryosphere system to short eccentricity modulation of climatic precession. In contrast, the responses of the global (high-latitude) climate system, cryosphere, and carbon cycle to the 405-kyr cycle, as expressed in benthic $\delta^{18}O$ and especially $\delta^{13}C$ signals, are more pronounced during ~2.4-Myr minima. The relationship between the recurrent episodes of high-amplitude ~110-kyr $\delta^{18}O$ cycles and the ~1.2-Myr amplitude modulation of obliquity is not consistent through the Oligo-Miocene. Identification of these recurrent episodes at Walvis Ridge, and their pacing by the ~2.4-Myr eccentricity cycle, revises the current understanding of the main climate events of the Oligo-Miocene.

1. Introduction

The early Oligocene–early Miocene Epoch (here referred to as "Oligo-Miocene") constitutes the earliest phase of Earth's Cenozoic Icehouse, characterised by a continental-size ice-cap on Antarctica

* Corresponding author.
E-mail address: diederik.liebrand@noc.soton.ac.uk (D. Liebrand).

http://dx.doi.org/10.1016/j.epsl.2016.06.007

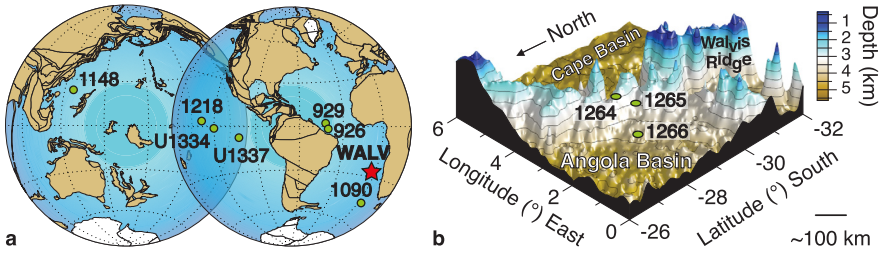

Fig. 1. Site locations. a) Palaeogeography (~23 Ma) showing approximate locations of the drill-sites discussed (www.odsn.de). The existence of a significant northern hemisphere Oligo-Miocene ice sheet is currently unknown. WALV stands for Walvis Ridge. b) Modern day bathymetry of the Walvis Ridge with selected ODP Leg 208 sites used in this study (Zachos et al., 2004 and references therein).

(Zachos et al., 1992; Coxall et al., 2005). Superimposed on secular trends, Earth's high-latitude climate system, cryosphere, and carbon cycle responded to astronomically forced changes in insolation during the Oligo-Miocene on time-scales ranging from 10s to 100s of thousands of years (kyr) (e.g. Pälike et al., 2006b). However, seasonal changes in insolation are affected by very long-period amplitude modulations of obliquity and precession that occur on million-year (Myr) time scales and are thought to have also played a critical role in the occurrence of key palaeoclimatic events.

Over the past ~30 yrs, understanding of Oligo-Miocene climate history from a marine perspective has evolved as new records have become available and new proxy records have been developed. Early interpretations of the Oligo-Miocene climate system were based on relatively low-resolution deep-sea stable isotope records and were described as a series of Oi and Mi oxygen isotope zones, marked by a maximum $\delta^{18}O$ value at their base (Miller et al., 1991; Wright and Miller, 1992). These $\delta^{18}O$ maxima are often referred to as Oi and Mi "events". As higher resolution records have become available it has become clear that, similar to the Plio-Pleistocene, climate change during the Oligo-Miocene is strongly paced by variations of Earth's eccentricity-modulated precession and obliquity cycles. The influence of long-period eccentricity and obliquity cycles (~2.4- and ~1.2-Myr, respectively) on the pacing of the cryosphere and carbon cycle is less well understood, although the prolonged absence of seasonal extremes (i.e. summer warming) may have played an important role in pacing global or high-latitude cooling and glacial expansion on Antarctica (Beaufort, 1994; Billups et al., 2004; Coxall et al., 2005; Lourens, 1994; Lourens and Hilgen, 1997; Pälike et al., 2006a, 2006b; Tian et al., 2008; Turco et al., 2001; Zachos et al., 2001). Records proximal to the Antarctic ice sheet provide support for astronomically controlled changes in seasonality having significantly affected high-latitude climate and the cryosphere (Naish et al., 2001).

Here, we present new high-resolution Oligo-Miocene (30.1–17.1 Ma) X-ray fluorescence (XRF) core scanning results and benthic $\delta^{13}C$ and $\delta^{18}O$ records from Ocean Drilling Program (ODP) Site 1264 on the Walvis Ridge, located in the southeastern Atlantic Ocean. This study builds on a previously published early Miocene stratigraphy from the same site (Liebrand et al., 2011). Time-series analysis, using an initial untuned magnetobiostratigraphic age model, indicates that eccentricity is the most strongly expressed of the astronomical parameters (Liebrand et al., 2011). We calibrate the records solely to the ~110-kyr component of the nominal (La2011_ecc3L) eccentricity solution and thereby avoid tuning complications arising from unknown phase relations and poorly constrained values for tidal dissipation and dynamical ellipticity that have affected tuning attempts based on obliquity and precession (Laskar et al., 2011; Zeeden et al., 2014). We construct a tuned age model by identifying the interference patterns resulting from different eccentricity periods (of mainly 95, 99, 124, 131 kyr/cycle and 405 kyr/cycle, here referred to as "~110-kyr" and "405-kyr" cycles) in signal and target curves and their subsequent alignment. We then use the eccentricity-tuned astrochronology from Site 1264 to evaluate existing interpretations of astronomical pacing of Oligo-Miocene records (Abels et al., 2007; Billups et al., 2004; Pälike et al., 2006a, 2006b; Tian et al., 2008; Zachos et al., 2001) and compare the results to those for the Miocene (Abels et al., 2005; Holbourn et al., 2013, 2015) and the Palaeocene–Eocene (Lourens et al., 2005). We specifically assess the influence of the very long period eccentricity (~2.4-Myr) and the long period obliquity (~1.2-Myr) cycles on the climate/cryosphere of the early phase of Earth's Cenozoic Icehouse.

2. Material and methods

2.1. Site descriptions

The records presented here are derived from two ODP Leg 208 sites drilled on the Walvis Ridge in the subtropical southeastern Atlantic Ocean (Fig. 1): Site 1264 (28°31.955′S, 2°50.730′E, 2505 m water depth) and Site 1265 (28°50.101′S, 2°38.354′E, 3059 m water depth) (Zachos et al., 2004). At Site 1264, two holes were drilled to ~280 m below sea floor (mbsf) that yielded relatively expanded Oligocene and Miocene strata. No clear primary palaeomagnetic signal was discerned in shipboard analysis (Bowles, 2006; Zachos et al., 2004), but we have transposed magnetostratigraphies to Site 1264 through detailed cross-site correlations with Sites 1265 and 1266 (28°32.550′S, 2°20.610′E, 3798 m water depth). Through these correlations four small recovery gaps in the Oligocene of Site 1264 are identified and filled with samples from Site 1265. Through comparison of integrated magnetobiostratigraphies, we compare stable isotope records and astrochronologies from the Walvis Ridge composite (primarily derived from Site 1264) to those from Ceara Rise Sites 926 and 929 (western equatorial Atlantic) (Pälike et al., 2006a), Agulhas Ridge Site 1090 (Atlantic sector of Southern Ocean) (Billups et al., 2004), Equatorial Pacific Sites 1218, U1334 and U1337 (Beddow et al., 2016; Holbourn et al., 2015; Pälike et al., 2006b) and South China Sea Site 1148 (Tian et al., 2008) (Fig. 1). Detailed site-to-site correlations of stable isotope records across the Oligocene–Miocene (Climatic) Transition (OMT) are presented in the supplementary information (Supp. Fig. S1) and in Beddow et al. (2016).

2.2. X-ray fluorescence core scanning

At Site 1264 the Oligo-Miocene study section is composed of $CaCO_3$-rich foraminifer-bearing nannofossil oozes (Zachos et al., 2004). XRF core scanning data were generated at the MARUM XRF-laboratory, University of Bremen. For Site 1264 the entire study interval was scanned along the shipboard splice with sufficient overlap between holes to enable independent splice review. Four splice gaps and/or uncertain tie-points were confirmed in the Oligocene part of the shipboard splice of Site 1264 (Fig. 2). To cover these intervals and check for stratigraphic continuity, we also scanned the lower Oligocene through lower Miocene of Site 1265. The XRF data were collected using an AVAATECH core scanner (Serial No. 12),

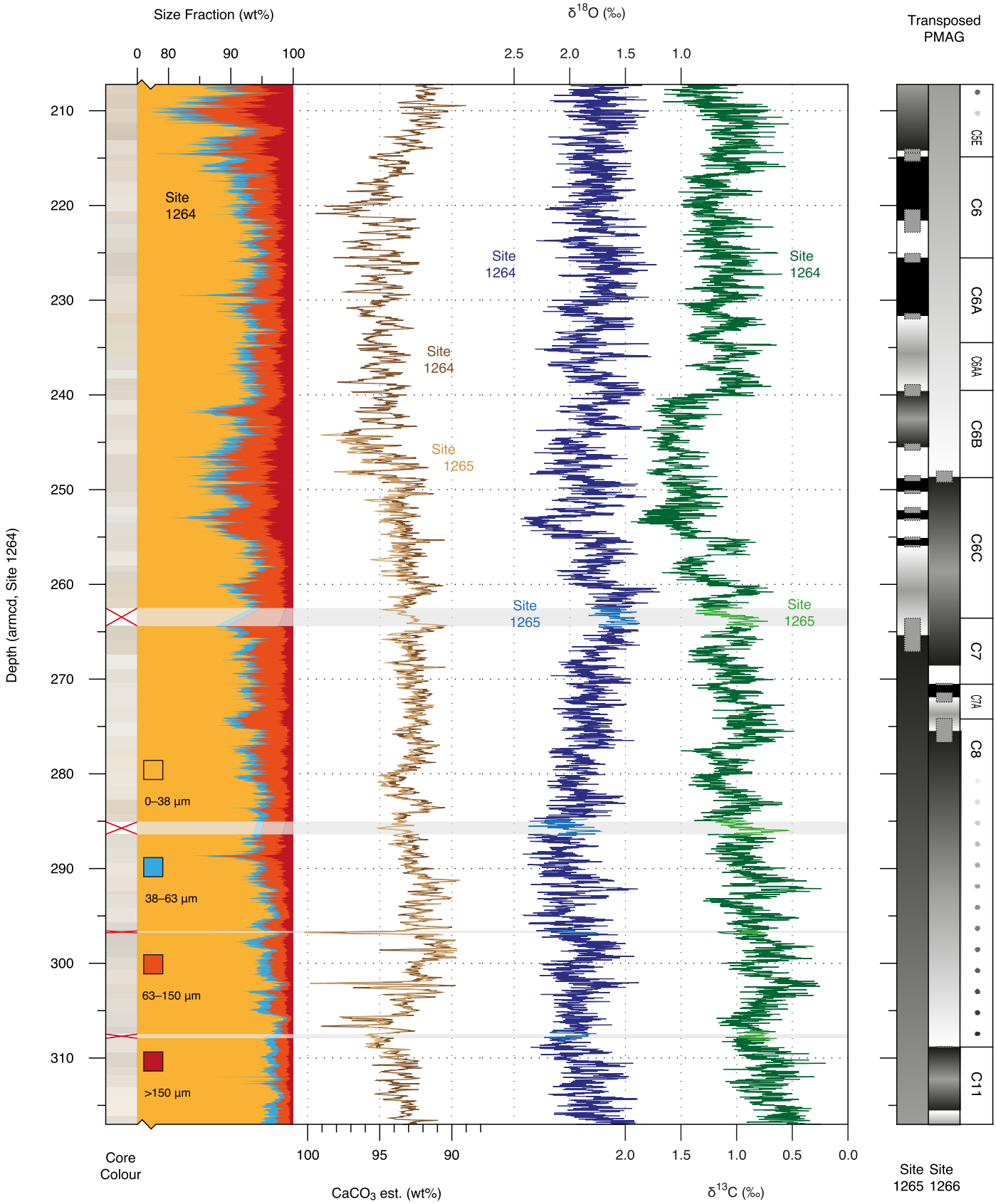

Fig. 2. Stratigraphic records from Sites 1264, 1265 and 1266. XRF and stable isotope depth-series are predominantly from Site 1264, complemented by data from Site 1265, which cover four small recovery gaps at Site 1264 (see red crosses and grey horizontal lines). Magnetostratigraphy is transposed from Sites 1265 and 1266 (Bowles, 2006). Grey indicates uncertain polarity, narrow grey bars indicate uncertain reversal positions. Core-photographs (Zachos et al., 2004) show apparent cyclicity resulting from uneven lighting conditions. We have therefore depicted colour-extracts of the well-lit parts from each core-section to graphically represent the general homogeneity of the mud. (For interpretation of the references to colour in this figure, the reader is referred to the web version of this article.)

fitted with an Oxford Instruments 100W Neptune Rh X-ray tube and a Canberra X-PIPS Silicon Drift X-ray Detector (SDD; Model SXD 15C-150-500). A step size of 20 mm, down-core slit size of 10 mm and a cross-core slit size of 12 mm were applied. The X-ray tube was operated at 10 kV with 0.15 mA current setting, and the measuring time for each step interval was 20 s with a dead time of >20 s. A processing model tailored to the 10 kV scans was applied. Outliers resulting from section-ends and cracks were identified by eye and removed. We use calibrations ($r^2_{(1264)} = 0.84$, $r^2_{(1265)} = 0.95$) between ln(Ca/Fe) and shipboard coulometric $CaCO_3$ measurements from Sites 1264 and 1265 (Zachos et al., 2004) to estimate $CaCO_3$ content continuously throughout the study interval (Supp. Fig. S2). "$CaCO_3$ est." is used throughout the text to refer to carbonate content estimated by ln(Ca/Fe). Gaps in the $CaCO_3$ est. record from Site 1264 were supplemented with data from Site 1265. The use of a log-ratio record is preferred over integrated elemental area or "count" records to avoid biases related to, for example, the closed sum effect (inherent to XRF core scanning) and variable grain-size and water content; the use of log ratios also aids the comparability between XRF data obtained from the different drill-sites and/or scanners (Weltje and Tjallingii, 2008).

2.3. Depth models and site-to-site correlations

The shipboard splices of Sites 1264 (between 206–316 mcd), 1265 (between 117–163 mcd) and 1266 (133–198 mcd) are revised here using shipboard magnetic susceptibility and colour reflectance data (Zachos et al., 2004) and new XRF data. For several splice tie-points, small corrections are made. The new composite depth scales are referred to as "revised meters composite depth" (rmcd). For all sites, we also present an adjusted-rmcd (armcd) scale to correlate intervals that fall outside the splice to the splice and hence, armcd is equivalent to rmcd in the intervals within the splice.

The spliced records are correlated in the depth domain between Walvis Ridge Sites 1264, 1265 and 1266 using visually selected multi-sensor track magnetic susceptibility, colour reflectance or XRF tie-points and subsequent automated correlation using the Match script (Lisiecki and Lisiecki, 2002). No significant changes are made for the previously published early Miocene correlation between Sites 1264 and 1265 (Liebrand et al., 2011). We estimate the maximum uncertainty in the depth correlations to be of the order of 10–20 cm, depending on the structure of the data in a particular interval.

2.4. Sample processing and stable isotope analyses

For this study, the previously published early Miocene record from Site 1264 (1919 samples spanning ~44 m between ~216 and 260 armcd, or ~5 Myr, Liebrand et al., 2011), was extended downwards into the Oligocene and upwards into the Miocene (2689 new samples, spanning ~67 m between ~207 and 216 armcd, and between ~260 and 318 armcd, or ~8 Myr in total). All new samples were taken at 2.5-cm resolution along the splice at a volume of 10–15 cm^3. Weights were recorded after each step of sample processing. Discrete sample magnetic susceptibility was measured on freeze-dried bulk samples at Utrecht University on a Kappabridge KLY-2 and at the University of Southampton on a Kappabridge KLY-4 magnetic susceptibility system. Samples were washed over 38, 63 and 150 µm sieves with tap water and dried overnight at 50 °C. For all samples, the epifaunal benthic foraminifer species *Cibicides mundulus* was picked from the >150 µm fraction. Stable isotope measurements were performed on single tests (i.e. the visually best specimen available per sample); however, two to four specimens were measured simultaneously in ca. 50% of the samples to reach the minimum (~20 µg) or ideal (30–50 µg) sample weight for the Kiel carbonate device. For the Site 1264 sample set ($n = 2536$), the foraminiferal calcite was reacted with phosphoric acid in a Thermo Finnigan Kiel-III automated preparation system at Utrecht University. Purified CO_2 was analysed on a Thermo Finnigan MAT 253 mass spectrometer. The results were compared to an internal gas standard and isotopic ratios were drift-corrected to nine individual NBS-19 values measured along each sample run. To cover the four gaps in the Oligocene part of the Site 1264 records, 153 samples of Site 1265 were measured using a Thermo Finnigan GasBench-II carbonate preparation device coupled to a Thermo Finnigan Delta-V mass spectrometer at Utrecht University. A small (0.2‰) correction was applied for the oxygen isotope results obtained on the Delta-V to match duplicate runs ($n = 27$) of the same sample set measured on the Thermo Finnigan MAT 253. Outliers defined in either the oxygen or carbon stable isotope records from Sites 1264 and 1265 were removed from both records and, if possible, remeasured. We also redefined outliers in the previously published early Miocene part of the records, which were measured at both Utrecht University and the University of Florida (Liebrand et al., 2011).

2.5. Time-series analysis

Power spectra of the depth- and time-series were calculated using Blackman–Tukey Fast-Fourier Transforms (Paillard et al., 1996). Wavelet analyses were applied to track cyclicities and to quantify their changing amplitudes through depth or time (Grinsted et al., 2004) and to calculate their mean spectral power (Torrence and Compo, 1998). The wavelet-script of Grinsted et al. (2004) was adapted to enable three-dimensional (3D) viewing, which enhanced the visual resolvability of the time-period transforms also when depicted in two dimensions (2D). To further assess the amplitude evolution of specific frequency bandwidths, broad bandwidth Gaussian filters (Paillard et al., 1996) and their Hilbert-transforms were computed. These results were compared in the age-domain to those of the astronomical calculations (Laskar et al., 2011). Blackman–Tukey cross-spectra were calculated between the data records and eccentricity to obtain coherency and phase estimates (Paillard et al., 1996).

3. Results

3.1. Description of the records

3.1.1. Size-fraction, XRF, and stable isotope records

The dry weights of the three sample fractions, combined with the dry weights of the washed samples, were used to calculate weight percent (wt%) records of the 0–38, 38–63, 63–150 and >150 µm size fractions (Fig. 2). At Site 1264, a steady increase in the percentage of the 63–150 µm fraction is observed between 305–250 armcd (late Oligocene), briefly interrupted by a small decrease between 260–255 armcd, which is followed by a steady decrease between 250–220 armcd and by another increase between 220–207 armcd (early Miocene). Peaks in the >150 µm size fraction are observed near 253 armcd (OMT interval) and 210 armcd. Higher wt% values in the >150 µm size fraction are recorded in the upper part of the study section between 253–207 armcd (early Miocene) compared to the lower study interval (317–253 armcd; mid to late Oligocene) (Fig. 2).

Variability in the XRF-derived $CaCO_3$ est. record ranges between 88 and 100 wt% $CaCO_3$ and is largest between 252–216 armcd (early Miocene) and 279–318 armcd (mid Oligocene) (Fig. 2). These intervals also record the highest and lowest $CaCO_3$ values in the study interval. Reduced variability is recorded between 252–279 armcd (late Oligocene).

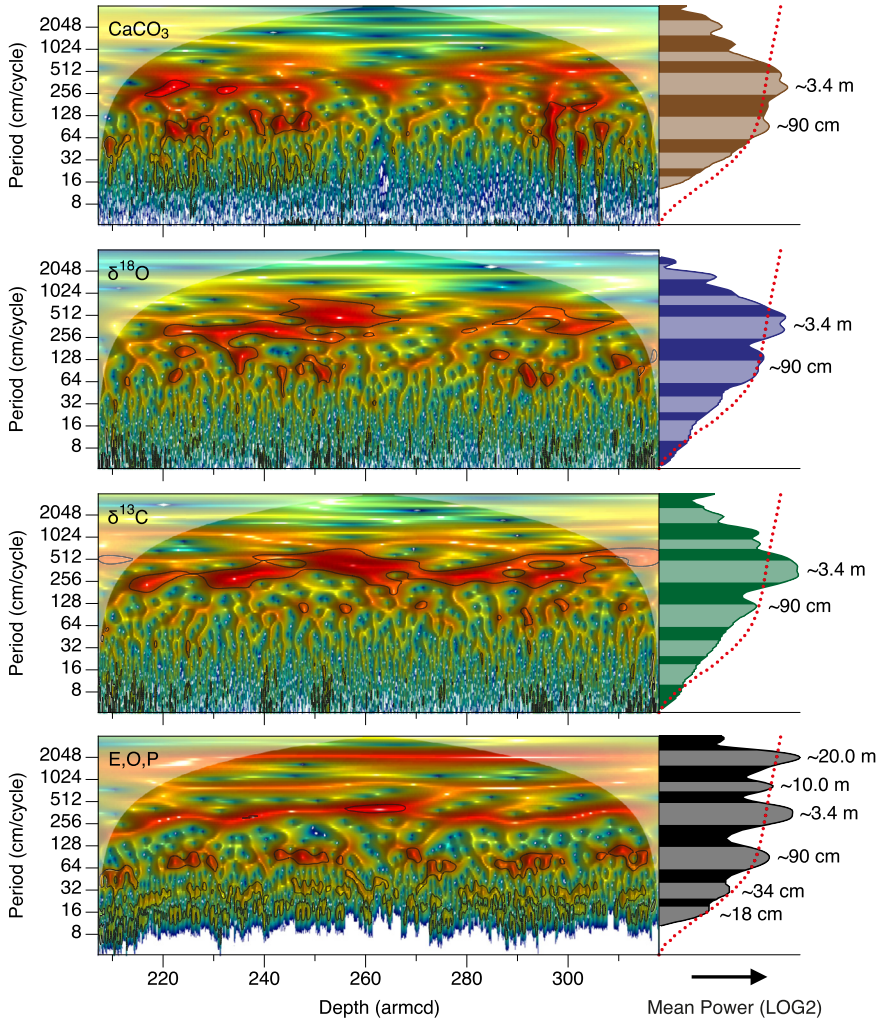

Fig. 3. Wavelet analyses in the stratigraphic domain. 2D views of 3D-wavelets (after Grinsted et al., 2004; Torrence and Compo, 1998). Continuous black lines on the wavelets represent the 95% significance levels. E, O, P stand for an arbitrary mix of eccentricity, obliquity, and precession (Laskar et al., 2011, 2004), which here is rescaled to depth using the tuning tie-points.

Benthic foraminiferal stable oxygen isotope ratios ($\delta^{18}O$) vary between 1.25 and 2.45‰, resulting in a total range of 1.2‰ across the study interval (Fig. 2). The highest $\delta^{18}O$ values of ~2.4‰ are reached at ~253 armcd (Oligocene–Miocene Transition). Low $\delta^{18}O$ values of ~1.2‰ are recorded in several intervals between ~263–220 armcd (latest Oligocene and early Miocene). After detrending, the $\delta^{18}O$ record has a standard deviation of ~0.15‰ and a maximum variability of ~1.0‰. Similar to the $CaCO_3$ est. record, an interval with particularly reduced amplitude variability in $\delta^{18}O$ is recorded between 260–280 armcd (late Oligocene).

Stable carbon isotope ratios ($\delta^{13}C$) of *C. mundulus* range between ~0.2 and ~1.9‰ throughout the record (Fig. 2). A long-term increase in $\delta^{13}C$ is observed up to 240 armcd, which is interrupted by a step-wise decrease at 240 armcd corresponding to the Oligocene–Miocene Carbon Maximum (Hodell and Woodruff, 1994). Several $\delta^{13}C$ minima of ~0.2‰ are recorded between 290–318 armcd. The $\delta^{13}C$ record peaks with values of ~1.9‰ at ~253 armcd. After the long-term trend is removed, the $\delta^{13}C$ record has a standard deviation of ~0.15‰ and shows ~1.0‰ amplitude variability.

3.1.2. Magnetostratigraphy

Despite recognition of clear polarity zones at nearby Deep-Sea Drilling Project (DSDP) Leg 73 sites (e.g. Tauxe and Hartl, 1997), it was not possible to generate a magnetostratigraphic record of similar quality at Site 1264 (Bowles, 2006; Zachos et al., 2004). To obtain magnetostratigraphic age constraints we instead transposed the palaeomagnetic records from Site 1265 (C5En(o)–C7n(y)) and Site 1266 (C6Cn.1n(y)–C11n.2n(o)) to Site 1264 (see Section 2.3). The chron labelling of Sites 1265 and 1266 is reinterpreted after comparison with the Oligocene and Miocene GPTS (Hilgen et al., 2012; Vandenberghe et al., 2012); the published magnetostratigraphies of these sites, however, have not been revised.

4. Cyclostratigraphy and tuned age model

4.1. Cyclostratigraphy

4.1.1. Spectral analysis in the depth-domain

Wavelet and mean spectral-power analyses were initially carried out on the proxy records in the depth domain. All depth series ($CaCO_3$ est., $\delta^{13}C$, $\delta^{18}O$) show at least two (broad) spectral peaks: the first peak centred at ~3.4 m/cycle and a second peak at ~0.9 m/cycles, of which the former is most strongly recorded in $\delta^{13}C$ and the latter in $CaCO_3$ est. and $\delta^{18}O$ (Fig. 3). We recognise clear bundling of three to four ~0.9 m cycles into ~3.4 m cycles in the best-preserved intervals of the $CaCO_3$ est. record (e.g. between 220–250 mcd, Fig. 2). In general, the spectral power of the shorter (<1 m/cycle) periods is much reduced compared to that of the longer (>1 m/cycle) periods. The ~3.4 m cycle in $\delta^{13}C$

can be tracked nearly continuously in the depth domain, suggesting that sedimentation rates for the largest part of the record were relatively stable and that spectral peaks in the depth domain are reliable indicators of periods in the age domain. The ~3.4 m/cycle period is split in two components between 285 and 315 armcd, indicating that two closely spaced periods are present. The strongest responses of both stable isotope records at the ~3.4 m/cycle period are present at ~255 armcd.

4.1.2. Application of initial magneto-biostratigraphic age model

An initial age model based on a polynomial fit through selected bio- and magnetostratigraphic age control points was applied to the Site 1264 record (Bowles, 2006; Zachos et al., 2004) (Supp. Fig. S3). This polynomial age model is not affected by transient changes in sedimentation rates or assumptions about astronomical climate forcing. Based on the initial age model, the bundling recognised in the $CaCO_3$ est. depth-series represents three to four ~110-kyr cycles (~0.9 m/cycle) into 405-kyr cycles (~3.4 m/cycle). Consequently, we confidently link the ~3.4 m and ~0.9 m cycles present throughout nearly all depth-series to 405- and ~110-kyr eccentricity periods, respectively. Wavelet depth-period conversions show that we can track the ~3.4 m and ~0.9 m (weaker) cycles and that these cycles vary moderately in thickness throughout the records (between 5–2 m and 1.5–0.5, respectively; Fig. 3).

4.1.3. Proxy for tuning and phase relationships

The $CaCO_3$ est. record is the most continuous recorder of the ~110-kyr eccentricity cycle throughout the study interval and is selected as tuning signal. We favour tuning to $CaCO_3$ est. over tuning to the isotope records, as the former likely represents a more direct regional response to insolation forcing, whereas the latter were most likely affected by the slow response times of the global cryosphere and carbon systems introducing phase lags. It is uncertain whether carbonate production or water column/seafloor dissolution was a more important control on carbonate accumulation at Site 1264, but identification of the dominant process is important because it determined the phase relation of the $CaCO_3$ est. record to eccentricity. The phase relationship between benthic foraminiferal $\delta^{18}O$ and eccentricity, however, is clear at Site 1264 and also at other drill sites (Pälike et al., 2006a, 2006b), with maxima in $\delta^{18}O$ (indicative of cooler more glacial conditions) associated with ~110-kyr eccentricity minima and *vice versa*. $\delta^{18}O$ and $CaCO_3$ est. are positively correlated throughout the Site 1264 record on the ~110-kyr period, and hence we infer that maxima in $CaCO_3$ correspond to minima in eccentricity (and *vice versa*). Additional indication of an anticorrelation between $CaCO_3$ est. and eccentricity is the cycle-shape of early Miocene ~110-kyr $CaCO_3$ cycles that show narrow peaks and broad troughs between 19.5 and 22.5 Ma (Fig. 4), thereby mimicking the inverse of the eccentricity solution, despite the fact that (post-)depositional processes can distort cycle shapes (Herbert, 1994). The increase in absolute $CaCO_3$ values during glacial maxima (i.e. ~110-kyr eccentricity minima) and the change in ~110-kyr cycle shapes during the early Miocene suggest that carbonate production is the most important control on the $CaCO_3$ record. If dissolution was the main control on $CaCO_3$, the opposite phase relationship would be expected (Herbert, 1994) with peak dissolution (and hence low $CaCO_3$ content) during glacial maxima in response to, for example, the intrusion of more corrosive bottom waters into the Atlantic Ocean (e.g. Pälike et al., 2006a) or comparable processes. During the Oligocene, dissolution may have had a somewhat stronger control on the record. However, $CaCO_3$ values remain high at Site 1264 throughout the study interval, and there is no evidence of similarly strong ~110-kyr cyclicity in the size fraction records that would indicate major dissolution. With the anticorrelation between $CaCO_3$ and eccentricity determined at the ~110-kyr period, we infer that this relationship is completely in phase because of the striking similarity in the shape of the excursions between signal and target (Fig. 4). This allows $CaCO_3$ est. maxima to be tied to eccentricity minima without introducing a lag for the entire span of the record.

4.2. Tuned age model

4.2.1. Tuning to stable eccentricity

The choice of the eccentricity solution as target curve for tuning was primarily driven by the exceptionally strong expression of eccentricity in the $CaCO_3$ est. and benthic stable isotope records in combination with the lack of strong obliquity and precession-controlled variability. A broad Gaussian filter of the detrended data plotted on the initial magnetobiostratigraphic age model, centred around the 405-kyr period, identified 32 cycles, indicating that the total duration of the time-series is ~13 Myr. Initial tuning tie-points in the data filters were selected at every 405-kyr maximum, corresponding to 405-kyr eccentricity minima. Next, all data sets ($CaCO_3$, $\delta^{18}O$, $\delta^{13}C$) were considered to visually identify the individual ~110-kyr cycles. Fine-tuning of the entire record to the (nominal) La2011_ecc3L eccentricity solution was, however, solely based on a synchronisation (i.e. final depth-to-age tie point selection) of $CaCO_3$ est. maxima to ~110-kyr eccentricity minima (hereafter referred to as the "tuned age model"). Eccentricity minima correspond to periods when Earth's orbit around the sun was near circular and form relatively short lasting "events" in the eccentricity solution (compared to the maxima), which makes them precise age-calibration points. The latest numerical eccentricity solution (La2011_ecc3L) is considered to be reliable back to ~50 Ma (Laskar et al., 2011). Application of the tuned age model across the Site 1264 study interval indicates that sedimentation rates range between ~0.5 and 1.5 cm/kyr (Supp. Fig. S4).

4.2.2. Spectral analysis in the tuned time-domain

On the astronomically tuned age model, the Site 1264 records span the interval between 30.1 and 17.1 Ma (Fig. 4). This comprises a Rupelian–Burdigalian interval contemporaneous with 405-kyr eccentricity Cycles 43–74 and Chrons C5–C11. It further encompasses ~2.4-Myr eccentricity Cycles 8–13 and ~1.2-Myr obliquity Cycles 16–26. Power-spectral and wavelet analyses of the eccentricity-tuned time-series of $CaCO_3$ est., $\delta^{13}C$, and $\delta^{18}O$ display high spectral power at the ~110- and 405-kyr eccentricity frequencies and low (or even absent) spectral power at the higher obliquity and precession frequencies (Fig. 5). Intervals with high-amplitude ~110-kyr power reoccur in the wavelet of $\delta^{18}O$ at ~29.4, ~27.4, ~22.8 and ~19.6 Ma. An additional low frequency spectral peak is recorded in $\delta^{18}O$ and $\delta^{13}C$ that corresponds to periods of ~160- and ~200-kyr, respectively; during eccentricity Cycle 53 a very high-amplitude response on this period can be observed in the $\delta^{18}O$ record. The 405-kyr cycles can be most easily tracked in the stable isotope records, despite the lack of a strong 405-kyr signal in some intervals. This shows time periods, particularly during ~2.4-Myr eccentricity maxima, where the relative response of the proxy records to 405-kyr eccentricity was much attenuated, for example, during the late Oligocene and (briefly) post-OMT (Fig. 5). The $CaCO_3$ est. record shows split ~125-kyr and ~95-kyr responses during ~2.4-Myr eccentricity maxima in the early Miocene, similar to the eccentricity solution.

4.2.3. Filtering and amplitude modulation

Detrended and normalised time-series were filtered using broad Gaussian band-pass filters centred on the 1/405 and 1/110 (combined 1/125 and 1/95) eccentricity frequencies (Paillard et al., 1996). Additionally, amplitude modulations of the filters were calculated using a Hilbert-transform (e.g. Shackleton et al., 1999).

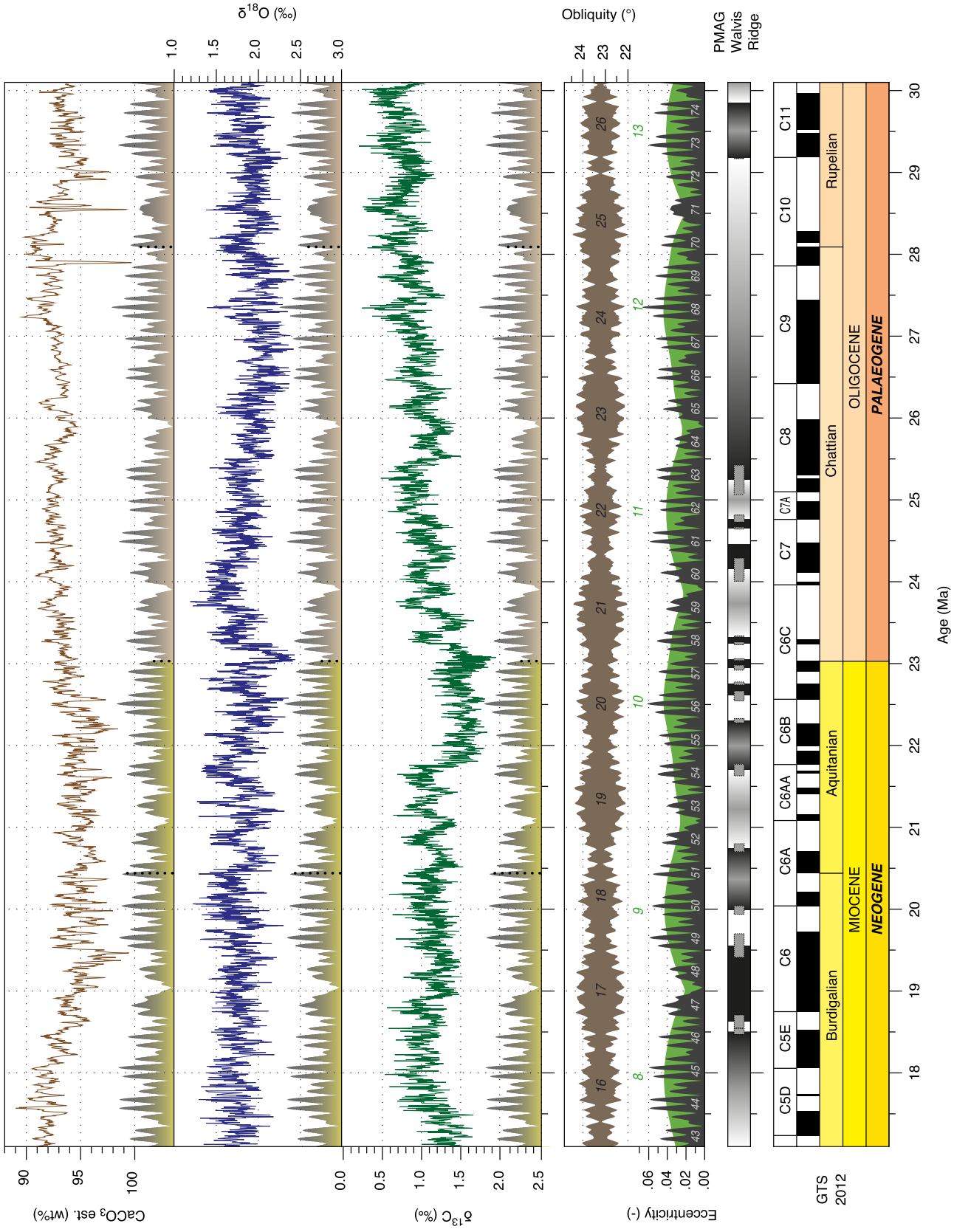

Fig. 4. Astrochronology from Walvis Ridge (predominantly Site 1264). Eccentricity-tuned records plotted against the stable components (i.e. modulations in case of obliquity) of the La2004 obliquity and La2011_ecc3L eccentricity solutions (Laskar et al., 2011, 2004). Green, black, and grey numbers represent the ~2.4-Myr eccentricity, ~1.2-Myr obliquity, and 405-kyr eccentricity cycles, respectively, counted back from the present. Note that obliquity is only depicted for comparison; it did not serve as tuning-target. The transposed (to Site 1264) and tuned magnetostratigraphies from Sites 1265 and 1266 (Bowles, 2006) are combined and compared to the GTS2012 (Hilgen et al., 2012; Vandenberghe et al., 2012). Grey means uncertain polarity, narrow grey bars represent uncertain reversal positions. (For interpretation of the references to colour in this figure, the reader is referred to the web version of this article.)

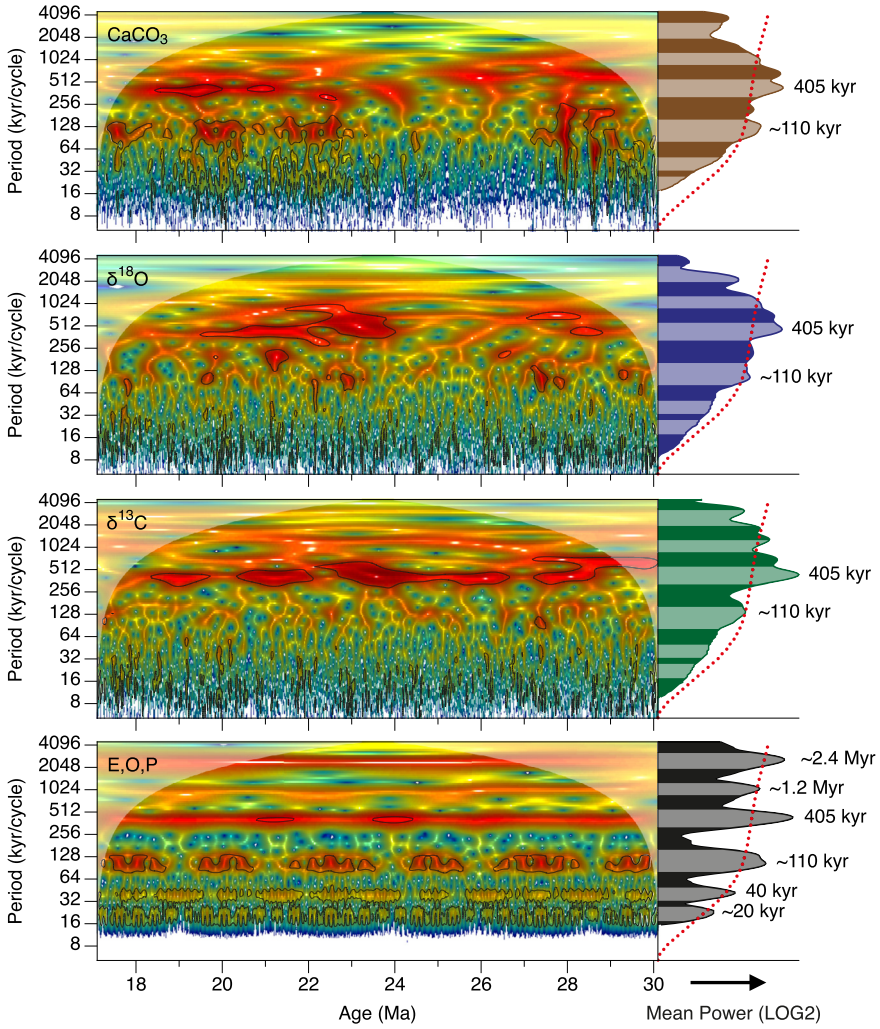

Fig. 5. Wavelet analyses in the tuned age domain. See Fig. 3 for explanation.

The amplitude of the 405-kyr cycle in $\delta^{13}C$ is largest during ~2.4-Myr minima, thereby mimicking the amplitude modulation of the 405-kyr filtered eccentricity solution, albeit slightly amplified and lagged in certain intervals (Fig. 6, Supp. Fig. S5). A similarly strong response is not observed in $\delta^{18}O$, but a weaker ~2.4-Myr modulation of 405-kyr cycles is still apparent, especially in the Oligocene interval. The $CaCO_3$ est. record does not show a clear 405-kyr amplitude response to ~2.4-Myr eccentricity. The amplitude modulation of the ~110-kyr cycle in $CaCO_3$ est., however, shows large responses during 405-kyr eccentricity Cycles 72, 69–68, 56–54, 50, 49 and 44 (Fig. 7). Similar analyses on $\delta^{18}O$ show strong ~110-kyr cycles concurrent with 405-kyr eccentricity Cycles 73, 69–68, 57 and 49. An attenuated amplitude response of $\delta^{18}O$ to the ~110-kyr eccentricity cycle corresponds to 405-kyr eccentricity Cycles 64–59. The $\delta^{13}C$ record shows strong ~110-kyr responses contemporaneous with 405-kyr eccentricity Cycles 69 and 43.

4.2.4. Coherency and phase

All time-series are coherent with eccentricity at the 405-, ~125- and ~95-kyr periods and $CaCO_3$ est. is also coherent on the (weak) ~50 kyr eccentricity period (Fig. 8). Spectral power and coherency are variable throughout the records in close relation to amplitude modulation by the ~2.4-Myr eccentricity cycle. Blackman–Tukey cross-spectral phase estimates indicate an unstable phase of $CaCO_3$ est., a ~7 kyr lead of $\delta^{18}O$, and a ~18 kyr lag of $\delta^{13}C$ relative to eccentricity at the 405-kyr period (Fig. 8). At the ~125-kyr period lags of ~2 kyr, ~6 kyr and ~7 (i.e. 4–10) kyr relative to eccentricity are calculated, for $CaCO_3$ est., $\delta^{18}O$, and $\delta^{13}C$, respectively. An in-phase relationship is identified at the ~95-kyr eccentricity period for $CaCO_3$ est., while for $\delta^{18}O$ and $\delta^{13}C$ this is a lag of ~6 kyr (4–8 and. 3–9 kyr, respectively). The in-phase relations found for $CaCO_3$ est. to eccentricity at the ~110-kyr period (i.e. the combined ~95- and ~125-kyr periods) are imposed on the record by the tuning assumptions. We note that these phase estimates are sensitive to relatively small changes in the tuned age model and represent averages of the entire time-series, and not all are stable throughout this time interval. Phase relationships to obliquity and precession are not calculated as they are excluded from the tuning target curve.

5. Implications of eccentricity tuned age model

5.1. Eccentricity prevalence

Despite the lack of strong precession and obliquity signals at Site 1264, eccentricity-paced variability is strong in comparison to previously published Oligo-Miocene stable isotope and $CaCO_3$ est. records. Even in intervals with the highest sedimentation rates (~1.5 cm/kyr, e.g. between 29.5 and 28.5 Ma, and 24.8 and 22.0 Ma; Fig. 5), where higher frequencies have a greater likelihood of being preserved, eccentricity is still prevalent over precession and obliquity. This suggests that the dominance of ec-

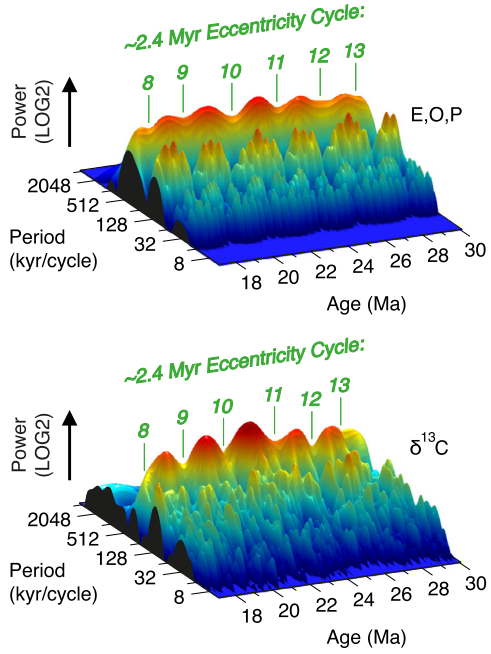

Fig. 6. ~2.4-Myr eccentricity amplitude modulation of the 405-kyr eccentricity cycle. 3D-wavelets show that the amplitude of the 405-kyr eccentricity cycle is largest during ~2.4-Myr eccentricity minima (Laskar et al., 2011). This is mimicked and amplified in the benthic $\delta^{13}C$ record. Green numbers corresponds to the ~2.4-Myr eccentricity cycles. Note that long-period cycles (>1 Myr) have been removed from both records. (For interpretation of the references to colour in this figure, the reader is referred to the web version of this article.)

centricity does not result from diagenesis, bioturbation or other post-depositional biases.

There is a striking similarity between $CaCO_3$ est. and eccentricity patterns at Site 1264, especially during the early Miocene part of the record (Fig. 4). Eccentricity pattern recognition in the $CaCO_3$ est. record becomes more difficult across intervals that correspond to strong ~2.4-Myr eccentricity minima, characterised by a weaker expression of the ~110-kyr beat for the duration of one or two 405-kyr cycles. Within the ~2.4-Myr minima, fewer tie-points were selected for tuning and only those that are certain on either side of the ~2.4-Myr eccentricity minimum were used.

On the tuned age model, eccentricity is strongly expressed in the mean power spectra and wavelet analyses. Only a weak obliquity component can be identified in certain intervals – an important result considering the exclusion of obliquity from the tuning target curve. The relative weakness of the obliquity signal at Site 1264 is probably the result of the moderate-to-low sedimentation rates and contrasts markedly with the records from Ceara Rise Sites 926 and 929, which are characterised by high sedimentation rates of ~2.5 cm/kyr and show a very strong imprint of obliquity (Pälike et al., 2006a). The phase-relations of the $CaCO_3$ est. and stable isotope records to the 405-kyr and ~110-kyr eccentricity periods at Site 1264, however, are in general agreement with those described for records from the Ceara Rise (Pälike et al., 2006a; Zachos et al., 2001) and the equatorial Pacific (Pälike et al., 2006b), with the exception of the apparent ~7-kyr lead of the Site 1264 $\delta^{18}O$ record to the 405-kyr eccentricity cycle, and the ~20- and ~30-kyr lags of the Ceara Rise $\delta^{18}O$ and $\delta^{13}C$ isotope chronologies, respectively, to the ~110-kyr eccentricity periods (Pälike et al., 2006a).

The 160–200 kyr period found in the time-series and power spectra of the isotope records (especially in $\delta^{18}O$) from Site 1264 may reflect (i) a response to the ~180-kyr modulation of the 40-kyr obliquity cycle, (ii) a harmonic response to two ~110-kyr eccentricity cycles, or (iii) a harmonic response to half of the 405-kyr eccentricity cycle. Whichever mechanism is responsible for this cyclicity, all possible mechanisms would require a non-linear climatic response, as no equally strong direct responses to obliquity or climatic precession are found in the power-spectra and wavelet analyses of Site 1264. The ~180-kyr period is also recognised in the amplitude modulation of spliced magnetic susceptibility records from Ceara Rise (Shackleton et al., 1999) and in power spectra of an (obliquity-tuned) early Miocene benthic stable isotope record from Site 1148 (Tian et al., 2008), suggesting that it may represent a global signal.

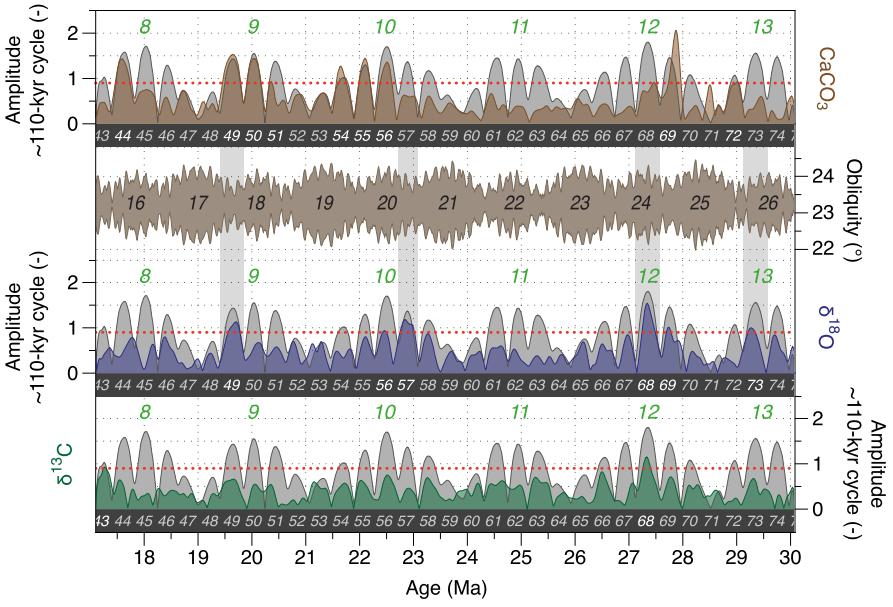

Fig. 7. 405-kyr eccentricity amplitude modulation of the ~110-kyr eccentricity cycle. Hilbert-transforms of detrended, normalised, and Gaussian filtered data (coloured) and eccentricity (grey; Laskar et al., 2011). The ~2.4-Myr and 405-kyr eccentricity cycle numbers are given in green and grey respectively. Red dotted line represents an arbitrary threshold value at half of the maximum eccentricity amplitude variability, selected to aid the eye in identifying 405-kyr cycles with particularly high-amplitude ~110-kyr responses. The episodes of high-amplitude ~110-kyr cyclicity in the $\delta^{18}O$ record are compared to the amplitude modulation of obliquity (dark grey area and black numbers; Laskar et al., 2004). (For interpretation of the references to colour in this figure, the reader is referred to the web version of this article.)

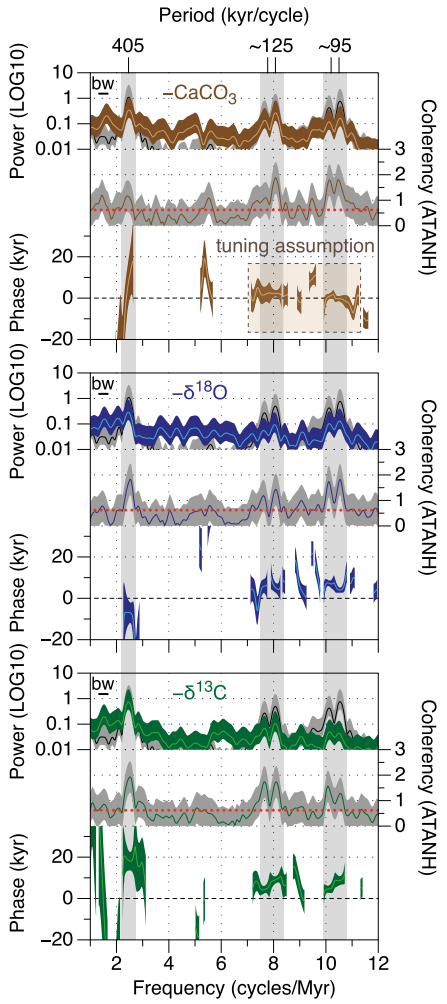

Fig. 8. Phase relationships with respect to eccentricity. Blackman–Tukey power-spectra, of the data records (coloured) versus eccentricity (grey; Laskar et al., 2011) and their combined cross-spectral coherency and phase estimates (Paillard et al., 1996). bw stands for bandwidth. ATANH stands for hyperbolic arctangent. Error bars and red dotted lines indicate the 95% confidence levels and coherency significance thresholds, respectively. The in-phase relation (~0 kyr) between $CaCO_3$ est. and eccentricity results from the tuning assumption. Negative phases correspond to a lead of the data with respect to eccentricity; positive phases represent a lag of the data to eccentricity. (For interpretation of the references to colour in this figure legend, the reader is referred to the web version of this article.)

5.2. Exclusion of precession and obliquity

Precession and obliquity were excluded from the Site 1264 tuning approach mainly due to the lack of a clear expression of these high-frequency signals. In addition, there are currently no constraints for tidal dissipation and dynamical ellipticity, which in turn affect the exact ages of individual obliquity and precession cycles (though not their modulations) beyond ~10 Ma (Zeeden et al., 2014). The eccentricity-based tuning approach applied in this study is unaffected by these problems but compromises age precision at the obliquity/precession level (~20–40 kyr). We argue, however, that previously published Oligo-Miocene age-calibration studies that incorporated obliquity and/or precession in their tuning-targets cannot guarantee age precision at this level either. The accuracy of any tuned ages >10 Ma is primarily constrained by the stable eccentricity solution (Zeeden et al., 2014), which modulates precession, or by tuning to the stable modulation of obliquity (Shackleton et al., 1999).

The weak imprints of precession and obliquity on the $CaCO_3$ est. and stable isotope records at Site 1264 could be the result of under-sampling, but only within the intervals with the lowest sedimentation rates. Technically, though, the sampling resolution of 2.0–2.5 cm (≤3.0 kyr) is above the Nyquist frequencies of precession and obliquity even in intervals with lower sedimentation rates. We propose several alternative mechanisms that may have affected the strength of precession and obliquity in the data. First, bioturbation and physical processes could have resulted in severe sediment mixing over time, which would have operated as a low-pass filter. Second, diagenesis resulting from partial $CaCO_3$ dissolution and recrystallization could have disturbed the higher frequency signals. 'Frosty' preservation of foraminifera (Sexton et al., 2006) at Site 1264 indicates some degree of diagenesis. Third, a precession signal could have been cancelled out in globally integrated proxy records if an equal and out-of-phase northern hemisphere and southern hemisphere ice-sheet response to precession forcing operated during the Oligo-Miocene interval, similar to what has been proposed for the 40-kyr obliquity-paced early Pleistocene (Raymo et al., 2006). Fourth, transient two-to-three fold changes in sedimentation rates (0.5–1.5 cm/kyr) across the study interval (Supp. Fig. S4) may have distorted the higher frequencies in the depth domain, so that the precession, obliquity and eccentricity components overlap in mean spectral power (Fig. 2, bottom panel) and especially the precession frequencies become harder to register (Herbert, 1994). Fifth, the strength of the eccentricity signal may have been enhanced relative to those of precession and obliquity, as the latter are not included in the tuning target curve. Sixth, there was a general lack of cyclicity in bottom-water temperature, carbonate production, etc. on obliquity/precessional time scales at Site 1264. It is likely that some combination of these mechanisms explains the weak imprint of precession and obliquity at Site 1264, with the exception of an out-of-phase precession control on Oligo-Miocene global land-ice since there is no evidence for an extensive NH ice sheet until the Plio-Pleistocene (Bailey et al., 2013).

5.3. Sedimentation rates and size fractions

Linear sedimentation rates (LSR) documented at Site 1264 (~0.5–1.5 cm/kyr) are typical for $CaCO_3$ dominated pelagic sites (Supp. Fig. S4). Peak LSR (~1.0–1.5 cm/kyr) are recorded across the OMT, contemporaneous with an increase in % coarse fraction (mainly within size fractions 63–150 μm and >150 μm; Fig. 2). The 63–150 μm size fraction increases between 27.5 and 23.0 Ma and then declines between 23.0 and 21.5 Ma. We link these trends to changing climatic and ecological conditions associated with the late Oligocene warming trend (~26.5–23.5 Ma; Fig. 4) and OMT (~23.5–22.5 Ma) that enhanced planktic foraminiferal production/accumulation. However, we cannot rule out a possible control of secular changes in carbonate saturation state and transient lysocline migrations on the preservation of planktic foraminifera. We note that the size fractions are selected based on the mesh size of the sieves and that they may also have been affected by changes in the production/accumulation of fine-fraction (nannofossil) carbonate. The increase in LSR across the OMT is synchronous with increased benthic foraminiferal accumulation rates at Site 1265 (Diester-Haass et al., 2011) and may indicate (temporarily) increased export productivity at Walvis Ridge during the OMT, perhaps associated with increased carbon burial in the deep sea acting as a contributing positive feedback to the transient OMT glaciation (Diester-Haass et al., 2011; Mawbey and Lear, 2013).

5.4. Age model comparison through magneto-biostratigraphy

The magnetostratigraphic records compiled here (Bowles, 2006) on an astronomically tuned age model may not be sufficiently resolved to further constrain the GPTS ages for polarity reversals

Table 1
Tuned chron ages from Walvis Ridge compared to the GTS2012 (Hilgen et al., 2012; Vandenberghe et al., 2012). Uncertainty intervals between top and bottom reflect the uncertain stratigraphic position at Sites 1265 and 1266. Uncertainties resulting from site-to-site correlation and astronomical tuning are not incorporated.

Chron	GTS2012 age (Ma)	WALV. Top tuned age (Ma)	WALV. Mid tuned age (Ma)	WALV. Bottom tuned age (Ma)	Δ GTS2012 – WALV. Mid tuned (kyr)
C5En (o)	18.524	18.469	18.497	18.540	27
C6n (y)	18.748	18.550	18.636	18.707	112
C6n (o)	19.722	19.413	19.535	19.701	187
C6An.1n (y)	20.040	19.937	19.979	20.037	61
C6An.2n (o)	20.709	20.704	20.765	20.799	−56
C6AAr.2n (y)	21.659	21.629	21.691	21.767	−32
C6Bn.2n (o)	22.268	22.276	22.300	22.329	−32
C6Cn.1n (y)	22.564	22.548	22.608	22.664	−44
C6Cn.1n (o)	22.754	22.742	22.760	22.775	−6
C6Cn.2n (y)	22.902	22.920	22.944	22.979	−42
C6Cn.2n (o)	23.030	23.040	23.052	23.061	−22
C6Cn.3n (y)	23.233	23.232	23.247	23.264	−14
C6Cn.3n (o)	23.295	23.322	23.332	23.338	−37
C7n.2n (y)	24.109	24.007	24.169	24.287	−60
C7n.2n (o)	24.474	24.459	24.459	–	15
C7An (y)	24.761	24.643	24.654	24.662	107
C7An (o)	24.984	24.729	24.766	24.816	218
C8n.2n (y)	25.304	25.062	25.244	25.418	60
C11n.1n (y)	29.183	29.167	29.170	29.175	13
C11n.2n (o)	29.970	29.856	29.856	–	114

(Table 1, Supp. Fig. S6). However, the tuned ages from Walvis Ridge generally support the ages of Billups et al. (2004), Pälike et al. (2006b) and the GTS2012 (Hilgen et al., 2012; Vandenberghe et al., 2012) for the chrons between 30.1 and 17.1 Ma (chrons C5D through C11) within the uncertainties resulting from site-to-site correlations, astronomical tuning and the exact position of the reversals in depth. The ages for Chron 7 (with the exception of C7n.2n(o)), marked as "uncertain" by Bowles (2006), appear anomalously young compared to the ages of the GTS2012 and Cande and Kent (1995). Additionally, the tuned early Miocene ages between 23.5 and 20.5 Ma (chrons C6An.2n (o) through C7n.2n (y)) are consistently older than the GTS2012 ages by ~33 kyr, suggesting that the linear interpolation between the mid Miocene and the OMT age points used to calibrate the magnetostratigraphic reversal ages for the early Miocene underestimates the ages of these chrons (Table 1, Supp. Fig. S6) (Hilgen et al., 2012; Lourens et al., 2004). A detailed description of the calcareous nannofossil biostratigraphy and age constraints is presented in the supplementary information (see also Supp. Fig. S7).

6. A revised astronomical-pacing theory for the Oligo-Miocene

6.1. Long-period eccentricity-pacing of benthic $\delta^{18}O$ and $\delta^{13}C$

We identify four recurrent, 405-kyr long intervals at Site 1264 that are characterised by strong oscillations in benthic foraminiferal $\delta^{18}O$. These intervals occur in response to high-amplitude ~110-kyr eccentricity forcing and are contemporaneous with ~2.4-Myr eccentricity maxima (Cycles 13, 12, 10 and 9) and with relatively lower amplitude 405-kyr eccentricity maxima (Cycles 73, 68, 57 and 49, Figs. 4 and 9). These $\delta^{18}O$ events stand apart by their very large magnitude of oscillation (~1.0‰) occurring on timescales as short as ~110 kyr. For instance, during 405-kyr eccentricity Cycle 68, there is a very prominent interglacial–glacial cycle with a magnitude of ~1.0‰ – almost encompassing the range of $\delta^{18}O$ variability in the entire record in one ~110-kyr cycle. This range of variability may also have been present at higher frequencies during the Oligo-Miocene, however, the relatively low sedimentation rates at Site 1264 likely prevent their detection in the isotope records.

There is no consistent relationship through the Oligo-Miocene between the $\delta^{18}O$ events (hereafter identified by their corresponding 405-kyr cycle number) and the ~1.2-Myr amplitude modulation of obliquity. Episodes 73 and 68 correspond (broadly) to ~1.2-Myr obliquity maxima, while Episodes 57 and 49 correspond to nodes in the ~1.2-Myr amplitude modulation of obliquity (Figs. 4 and 7). The $\delta^{18}O$ record from Site 1264 therefore only partially supports the view that the power of ~110-kyr cycles increases during nodes in the amplitude modulation of obliquity (Abels et al., 2005; Holbourn et al., 2013; Pälike et al., 2006a, 2006b), which also has implications for the transient glaciation across the OMT. The long-term early Oligocene–early Miocene context that Site 1264 provides for the OMT, combined with reconstructions of atmospheric CO_2 levels (Beerling and Royer, 2011; Zhang et al., 2013), suggests that tectonic events and the long-term trends in CO_2 contributed significantly to the severity of the transient glaciation across OMT. Additional evidence of secular changes within the climate/cryosphere system comes from the observation that certain intervals with similar eccentricity configurations (weak 405-kyr maxima during ~2.4-Myr maxima) did not result in high-amplitude ~110-kyr cycles in benthic $\delta^{18}O$, for example during ~2.4-Myr eccentricity Cycle 11 in the late Oligocene (Figs. 4 and 7).

The ~2.4-Myr cycle is also pronounced in the modulation of the 405-kyr filtered $\delta^{13}C$ record (Fig. 6, Supp. Fig. S5). Comparison with other high-resolution stratigraphies from the Meso- and Cenozoic shows that 405-kyr carbon cycle variability is persistently controlled by the ~2.4-Myr eccentricity pacing from the Cretaceous (Sprovieri et al., 2013), through Palaeo-Eocene (Littler et al., 2014; Lourens et al., 2005) to (at least) the Oligo-Miocene (Boulila et al., 2012; Pälike et al., 2006b, this study). A ~2.4-Myr pacing in the Oligo-Miocene is also reported in lacustrine sediments of the Ebro basin (Valero et al., 2014) and in land mammal turnover rates (Van Dam et al., 2006).

6.2. Recurring episodes of high-amplitude, ~110-kyr cyclicity in benthic $\delta^{18}O$

The high-resolution record from Site 1264 demonstrates that high-amplitude, ~110-kyr-paced benthic $\delta^{18}O$ cycles are associated with ~2.4-Myr eccentricity maxima and provides a new picture of global climate change during the Oligo-Miocene. Previous studies have shown that high-amplitude ~110-kyr cycles are present throughout the Oligocene and Miocene (Holbourn et al., 2013, 2015; Pälike et al., 2006b; Zachos et al., 2001), but

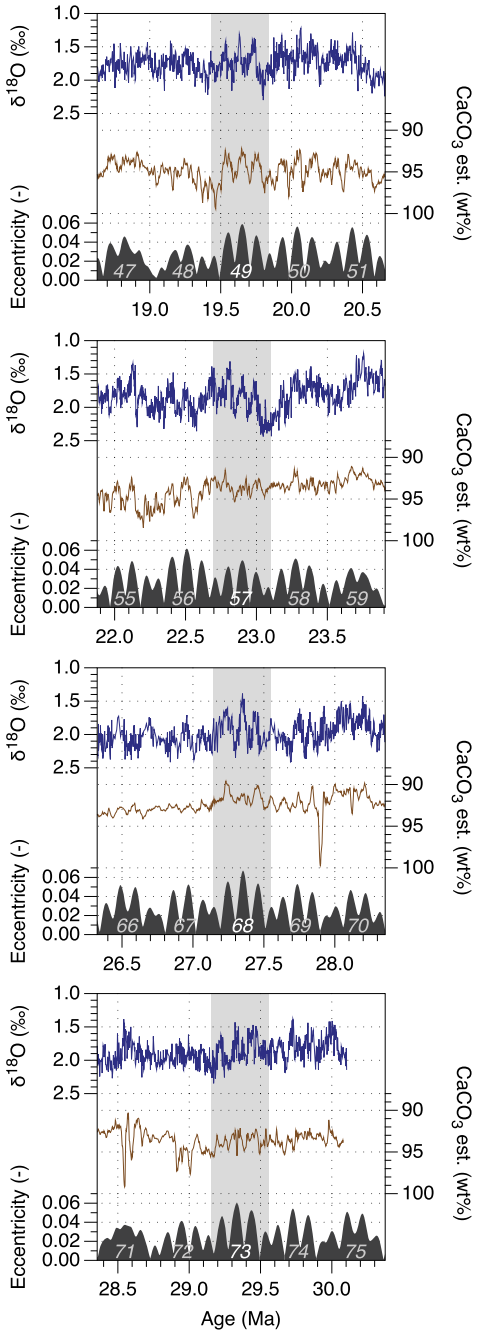

Fig. 9. Recurrent episodes of high-amplitude ~110-kyr cycles in $\delta^{18}O$. "History doesn't repeat itself, but it rhymes" (attributed to Mark Twain); "rhyming" climate/cryosphere histories, or natural experiments of Antarctic glaciation, of the Oligo-Miocene are shown. Grey numbers corresponds to 405-kyr eccentricity cycles.

the 13-Myr long record presented here gives a unique perspective on the recurrence of these high-amplitude cycles. We view the intervals of enhanced glacial/interglacial cyclicity (Episodes 73, 68, 57 and 49; Fig. 9) to be the most characteristic episodes of the Oligo-Miocene, in a similar way that hyperthermal events have come to define the key responses of interest of Cenozoic Greenhouse climate to eccentricity-paced carbon cycle perturbations (Lourens et al., 2005). This new view, based on a continuous high-resolution stratigraphy from one location spanning 13 Myr, represents a distinct improvement on the chemostratigraphic Oi and Mi zonation scheme originally defined based on low-resolution benthic $\delta^{18}O$ records (Miller et al., 1991; Wright and Miller, 1992). In that scheme, oxygen isotope zones were defined as 1.0 to 4.5 Myr long intervals with a positive $\delta^{18}O$ excursion at their base and were numbered, like biozones, in a chronological order. Later studies used these zonations to refer to the most prominent positive $\delta^{18}O$ excursions of the Oligocene and Miocene (e.g. Zachos et al., 1997). These positive $\delta^{18}O$ excursions have been previously postulated to occur at ~1.2-Myr intervals in conjunction with nodes in the amplitude modulation of obliquity (Lourens, 1994; Lourens and Hilgen, 1997; Pälike et al., 2006b; Turco et al., 2001; Zachos et al., 2001). The extended $\delta^{18}O$ record from Site 1264, with clear variability in the amplitude modulation of the ~110-kyr cycle, now shows that these recurrent episodes resulted from a nonlinear response of Earth's climate and cryosphere to ~2.4-Myr eccentricity pacing. This contrasts with an earlier interpretation of the untuned early Miocene interval of the same site, which proposed a pacing of glacial expansions in Antarctica and subsequent high-amplitude ~110-kyr variability in $\delta^{18}O$ as resulting from a nonlinear response to multiples of 405-kyr eccentricity cycles (Liebrand et al., 2011).

7. Conclusions

We present high-resolution XRF- and coulometry-based $CaCO_3$ and benthic foraminiferal $\delta^{18}O$ and $\delta^{13}C$ records from South Atlantic Ocean Site 1264 (Walvis Ridge) that span a 13-Myr interval through the early Oligocene to early Miocene (30.1 to 17.1 Ma). All time-series record a very strong imprint of eccentricity, particularly of short (~110-kyr) eccentricity. The dampened expression of obliquity and climatic precession may be regarded as atypical for Oligo-Miocene high-resolution climate proxy records but allows development of an age model solely based on the alignment with the eccentricity solution. This age calibration approach is further strengthened by the unknown phase relationship of the global climatic response to precession forcing and by the poorly constrained values for tidal dissipation and dynamical ellipticity during the Oligo-Miocene, which affect both the stability of obliquity and precession in the astronomical solutions. The eccentricity-based tuning of ODP Site 1264 is broadly in agreement with earlier astronomical age calibration studies and within error of GPTS2012 age calibrations of palaeomagnetic reversals.

The Site 1264 records show variable amplitudes of response to eccentricity forcing. The ~110 and 405-kyr responses are especially amplified and paced by the ~2.4-Myr eccentricity cycle. This view of pacing of the global climate system and the Antarctic ice sheet, controlled mainly by eccentricity modulation of precession during the mid Cenozoic, revises previous Oligo-Miocene astronomical pacing and forcing theories that attributed stronger and almost singular linear control of obliquity (and precession) on global change. The $\delta^{18}O$ data show that the global (high-latitude) Oligo-Miocene ocean–atmosphere–cryosphere system was modulated by the ~2.4-Myr very long period eccentricity cycle and remarkably sensitive on a timescale of ~110-kyr.

Acknowledgements

We like to thank Ian Croudace, Jan Drenth, Walter Hale, Geert Ittman, Samantha Gibbs, Yuxi Jin, Dominika Kasjaniuk, Daniel Kelly, Alice Lefebvre, David Naafs, Ursula Röhl, Eelco Rohling, Richard Smith, Megan Spencer, Anastasia Tsiola, Natasja Welters, Thomas Westerhold, Alex Wülbers, Andrew Yool, and Christian Zeeden for their help and for insightful discussions. This research used data acquired at the XRF Core Scanner Lab at the MARUM – Center for Marine Environmental Sciences, University of Bremen, Germany, supported by the DFG-Leibniz Center for Surface Process

and Climate Studies at the University of Potsdam. We used samples provided by the Ocean Drilling Program, sponsored by the US National Science Foundation and participating countries under the management of the Joint Oceanographic Institutions. This research has been made possible by funding of ERC grants 215458 and 617462, NWO grants 864.02.007 and 865.10.001, and NERC grant NE/K014137/1. All data presented in this paper are available online (www.pangaea.de).

Appendix A. Supplementary material

Supplementary material related to this article can be found online at http://dx.doi.org/10.1016/j.epsl.2016.06.007.

References

Abels, H.A., Hilgen, F.J., Krijgsman, W., Kruk, R.W., Raffi, I., Turco, E., Zachariasse, W.J., 2005. Long-period orbital control on middle Miocene global cooling: integrated stratigraphy and astronomical tuning of the Blue Clay Formation on Malta. Paleoceanography 20.

Abels, H.A., Van Simaeys, S., Hilgen, F., De Man, E., Vandenberghe, N., 2007. Obliquity-dominated glacio-eustatic sea level change in the early Oligocene: evidence from the shallow marine siliciclastic Rupelian stratotype (Boom Formation, Belgium). Terra Nova 19, 65–73.

Bailey, I., Hole, G.M., Foster, G.L., Wilson, P.A., Storey, C.D., Trueman, C.N., Raymo, M.E., 2013. An alternative suggestion for the Pliocene onset of major northern hemisphere glaciation based on the geochemical provenance of North Atlantic Ocean ice-rafted debris. Quat. Sci. Rev. 75, 181–194.

Beaufort, L., 1994. Climatic importance of the modulation of the 100 kyr cycle inferred from 16 m.y. long Miocene records. Paleoceanography 9, 821–834.

Beddow, H.M., Liebrand, D., Sluijs, A., Wade, B.S., Lourens, L.J., 2016. Global change across the Oligo-Miocene transition: high-resolution stable isotope records from IODP Site U1334 (equatorial Pacific Ocean). Paleoceanography 31, 81–97.

Beerling, D.J., Royer, D.L., 2011. Convergent Cenozoic CO_2 history. Nat. Geosci. 4, 418–420.

Billups, K., Pälike, H., Channell, J.E.T., Zachos, J., Shackleton, N.J., 2004. Astronomic calibration of the late Oligocene through early Miocene geomagnetic polarity time scale. Earth Planet. Sci. Lett. 224, 33–44.

Boulila, S., Galbrun, B., Laskar, J., Pälike, H., 2012. A ~9 Myr cycle in Cenozoic $\delta^{13}C$ record and long-term orbital eccentricity modulation: is there a link? Earth Planet. Sci. Lett. 317–318, 273–281.

Bowles, J., 2006. Data report: revised magnetostratigraphy and magnetic mineralogy of sediments from Walvis Ridge, Leg 208. In: Kroon, D., Zachos, J.C., Richter, C. (Eds.), Proc. Ocean Drill. Program Sci. Results, vol. 208. Ocean Drilling Program, College Station, TX.

Cande, S.C., Kent, D.V., 1995. Revised calibration of the geomagnetic polarity timescale for the Late Cretaceous and Cenozoic. J. Geophys. Res. 100, 6093–6095.

Coxall, H.K., Wilson, P.A., Pälike, H., Lear, C.H., Backman, J., 2005. Rapid stepwise onset of Antarctic glaciation and deeper calcite compensation in the Pacific Ocean. Nature 433 (7021), 53–57.

Diester-Haass, L., Billups, K., Emeis, K., 2011. Enhanced paleoproductivity across the Oligocene/Miocene boundary as evidenced by benthic foraminiferal accumulation rates. Palaeogeogr. Palaeoclimatol. Palaeoecol. 302, 464–473.

Grinsted, A., Moore, J.C., Jevrejeva, S., 2004. Application of the cross wavelet transform and wavelet coherence to geophysical time series. Nonlinear Process. Geophys. 11, 561–566.

Herbert, T.D., 1994. Reading orbital signals distorted by sedimentation: models and examples. Spec. Publs Int. Ass. Sediment 19, 483–507.

Hilgen, F.J., Lourens, L.J., van Dam, J.A., 2012. The Neogene period. In: Gradstein, F.M., Ogg, J.G., Schmitz, M., Ogg, G.M. (Eds.), The Geologic Time Scale 2012. Elsevier.

Hodell, D.A., Woodruff, F., 1994. Variations in the strontium isotopic ratio of seawater during the Miocene: stratigraphic and geochemical implications. Paleoceanography 9, 405–426.

Holbourn, A., Kuhnt, W., Clemens, S., Prell, W., Andersen, N., 2013. Middle to late Miocene stepwise climate cooling: evidence from a high-resolution deep-water isotope curve spanning 8 million years. Paleoceanography 28, 688–699.

Holbourn, A., Kuhnt, W., Kochhann, K.G.D., Andersen, N., Meier, K.J.S., 2015. Global perturbation of the carbon cycle at the onset of the Miocene Climatic Optimum. Geology 43 (2), 123–126.

Laskar, J., Gastineau, M., Delisle, J.-B., Farrés, A., Fienga, A., 2011. Strong chaos induced by close encounters with Ceres and Vesta. Astron. Astrophys. 532, 1–4.

Laskar, J., Robutel, P., Joutel, F., Gastineau, M., Correia, A.C.M., Levrard, B., 2004. A long-term numerical solution for the insolation quantities of the Earth. Astron. Astrophys. 428, 261–285.

Liebrand, D., Lourens, L.J., Hodell, D.A., De Boer, B., Van de Wal, R.S.W., Pälike, H., 2011. Antarctic ice sheet and oceanographic response to eccentricity forcing during the early Miocene. Clim. Past 7, 869–880.

Lisiecki, L.E., Lisiecki, P.A., 2002. Application of dynamic programming to the correlation of paleoclimate records. Paleoceanography 17.

Littler, K., Röhl, U., Westerhold, T., Zachos, J.C., 2014. A high-resolution benthic stable-isotope record for the South Atlantic: implications for orbital-scale changes in Late Paleocene–Early Eocene climate and carbon cycling. Earth Planet. Sci. Lett. 401, 18–30.

Lourens, L.J., 1994. Astronomical Forcing of Mediterranean Climate During the Last 5.3 Million Years. Institute of Earth Sciences, Department of Geology, Utrecht University, Utrecht, p. 247.

Lourens, L.J., Hilgen, F.J., 1997. Long-periodic variations in the earth's obliquity and their relation to third-order eustatic cycles and late Neogene glaciations. Quat. Int. 40, 43–52.

Lourens, L.J., Hilgen, F.J., Shackleton, N.J., Laskar, J., Wilson, D., 2004. The Neogene period. In: Gradstein, F., Ogg, J., Smith, A. (Eds.), A Geologic Time Scale 2004. Cambridge University Press.

Lourens, L.J., Sluijs, A., Kroon, D., Zachos, J.C., Thomas, E., Röhl, U., Bowles, J., Raffi, I., 2005. Astronomical pacing of late Palaeocene to early Eocene global warming events. Nature 435, 1083–1087.

Mawbey, E.M., Lear, C.H., 2013. Carbon cycle feedbacks during the Oligocene–Miocene transient glaciation. Geology 41 (9), 963–966.

Miller, K.G., Wright, J.D., Fairbanks, R.G., 1991. Unlocking the ice house: Oligocene–Miocene oxygen isotopes, eustacy and margin erosion. J. Geophys. Res. 96, 6829–6848.

Naish, T.R., Woolfe, K.J., Barrett, P.J., Wilson, G.S., Atkins, C., Bohaty, S.M., Bücker, C.J., Claps, M., Davey, F.J., Dunbar, G.B., Dunn, A.G., Fielding, C.R., Florindo, F., Hannah, M.J., Harwood, D.M., Henrys, S.A., Krissek, L.A., Lavelle, M., van der Meer, J., McIntosh, W.C., Niessen, F., Passchier, S., Powell, R.D., Roberts, A.P., Sagnotti, L., Scherer, R.P., Strong, C.P., Talarico, F., Verosub, K.L., Villa, G., Watkins, D.K., Webb, P.-N., Wonik, T., 2001. Orbitally induced oscillations in the East Antarctic ice sheet at the Oligocene/Miocene boundary. Nature 413, 719–723.

Paillard, D., Labeyrie, L., Yiou, P., 1996. AnalySeries, Macintosh program performs time-series analysis. Eos 77, 379.

Pälike, H., Frazier, J., Zachos, J.C., 2006a. Extended orbitally forced palaeoclimatic records from the equatorial Atlantic Ceara Rise. Quat. Sci. Rev. 25, 3138–3149.

Pälike, H., Norris, R.D., Herrle, J.O., Wilson, P.A., Coxall, H.K., Lear, C.H., Shackleton, N.J., Tripati, A.K., Wade, B.S., 2006b. The heartbeat of the Oligocene climate system. Science 314, 1894–1898.

Raymo, M.E., Lisiecki, L.E., Nisancioglu, K., 2006. Plio-Pleistocene ice volume, Antarctic climate, and the global $\delta^{18}O$ record. Science 313.

Sexton, P.F., Wilson, P.A., Pearson, P.N., 2006. Microstructural and geochemical perspectives on planktic foraminiferal preservation: "Glassy" versus "Frosty". Geochem. Geophys. Geosyst. 7.

Shackleton, N.J., Crowhurst, S.J., Weedon, G.P., Laskar, J., 1999. Astronomical calibration of Oligocene–Miocene time. Philos. Trans. R. Soc., Math. Phys. Eng. Sci. 357, 1907–1929.

Sprovieri, M., Sabatino, N., Pelosi, N., Batenburg, S.J., Coccioni, R., Lavarone, M., Mazzola, S., 2013. Late Cretaceous orbitally-paced carbon isotope stratigraphy from the Bottaccione Gorge (Italy). Palaeogeogr. Palaeoclimatol. Palaeoecol. 379–380, 81–94.

Tauxe, L., Hartl, P., 1997. 11 million years of Oligocene geomagnetic field behaviour. Geophys. J. Int. 128, 217–229.

Tian, J., Zhao, Q., Wang, P., Li, Q., Cheng, X., 2008. Astronomically modulated Neogene sediment records from the South China Sea. Paleoceanography 23.

Torrence, C., Compo, G.P., 1998. A practical guide to wavelet analyses. Bull. Am. Meteorol. Soc. 79.

Turco, E., Hilgen, F.J., Lourens, L.J., Shackleton, N.J., Zachariasse, W.J., 2001. Punctuated evolution of global climate cooling during the late middle to early late Miocene: high-resolution planktonic foraminiferal and oxygen isotope records from the Mediterranean. Paleoceanography 16, 405–423.

Valero, L., Garcés, M., Cabrera, L., Costa, E., Sáez, A., 2014. 20 Myr of eccentricity paced lacustrine cycles in the Cenozoic Ebro Basin. Earth Planet. Sci. Lett. 408, 183–193.

Van Dam, J.A., Abdul Aziz, H., Angeles Alvarez Sierra, M., Hilgen, F.J., van den Hoek Ostende, L.W., Lourens, L.J., Mein, P., van der Meulen, A.J., Pelaez-Campomanes, P., 2006. Long-period astronomical forcing of mammal turnover. Nature 443, 687–691.

Vandenberghe, N., Hilgen, F.J., Speijer, 2012. The Paleogene period. In: Gradstein, F.M., Ogg, J.G., Schmitz, M., Ogg, G.M. (Eds.), The Geologic Time Scale 2012. Elsevier.

Weltje, G.J., Tjallingii, R., 2008. Calibration of XRF core scanners for quantitative geochemical logging of sediment cores: theory and application. Earth Planet. Sci. Lett. 274, 423–438.

Wright, J.D., Miller, K.G., 1992. Miocene stable isotope stratigraphy, Site 747, Kerguelen Plateau. In: Proc. Ocean Drill. Program Sci. Results, vol. 120.

Zachos, J.C., Breza, J.R., Wise, S.W., 1992. Early Oligocene ice-sheet expansion on Antarctica: stable isotope and sedimentological evidence from Kerguelen Plateau, southern Indian Ocean. Geology 20, 569–573.

Zachos, J.C., Flower, B.P., Paul, H.A., 1997. Orbitally paced climate oscillations across the Oligocene/Miocene boundary. Nature 388, 567–570.

Zachos, J.C., Kroon, D., Blum, P., Bowles, J., Gaillot, P., Hasegawa, T., Hathorne, E.C., Hodell, D.A., Kelly, D.C., Jung, J.-H., Keller, S.M., Lee, Y.S., Leuschner, D.C., Liu,

H., Lohmann, K.C., Lourens, L.J., Monechi, S., Nicolo, M., Raffi, I., Riesselman, C., Röhl, U., Schellenberg, S.A., Schmidt, D., Sluijs, A., Thomas, D., Thomas, E., Vallius, H., 2004. In: Proc. Ocean Drill. Program Init. Repts., vol. 208. Ocean Drilling Program.

Zachos, J.C., Shackleton, N.J., Revenaugh, J.S., Palike, H., Flower, B.P., 2001. Climate response to orbital forcing across the Oligocene–Miocene boundary. Science 292, 274–278.

Zeeden, C., Hilgen, F.J., Hüsing, S.K., Lourens, L.J., 2014. The Miocene astronomical time scale 9–12 Ma: new constraints on tidal dissipation and their implications for paleoclimatic investigations. Paleoceanography 29, 296–307.

Zhang, Y.G., Pagani, M., Liu, Z., Bohaty, S., DeConto, R., 2013. A 40-million-year history of atmospheric CO_2. Philos. Trans. R. Soc. A 371.